Supporting information for

Shared Binding Mode of Perrottetinene and Tetrahydrocannabinol Diastereomers inside the CB1 Receptor May Incentivize Novel Medicinal Drug Design: Findings from an *in Silico* Assay

Matheus Henrique Reis[†], Deborah Antunes[‡*], Lucianna H. S. Santos[§], Ana Carolina Ramos Guimarães[‡], Ernesto Raul Caffarena[†]

[†]Grupo de Biofísica Computacional e Modelagem Molecular, Programa de Computação Científica, Fiocruz, Rio de Janeiro 21040-360, Brazil
[‡]Laboratório de Genômica Funcional e Bioinformática, Instituto Oswaldo Cruz, Fundação Oswaldo Cruz, Rio de Janeiro 21040-900, Brazil
[§]Laboratório de Modelagem Molecular e Planejamento de Fármacos, Departamento de Bioquímica e Imunologia, Instituto de Ciências Biológicas, Universidade Federal de Minas Gerais, Belo Horizonte 31270-901, Brazil.

*E-mail address: deborah.santos@fiocruz.br

Contents:

Figure S1. 2D diagrams of interactions of the best poses from redocking and cross-docking. 2

Figure S2. 2D diagrams of interactions of the best poses from docking. 3

Figure S3. Root mean square deviations of CB1R systems. 4

Table S1. Root mean square deviations (Å) of CB1R systems. 4

Figure S4. Root mean square deviations of PET systems during the equilibration stage (heavy atoms only). 5

Figure S5. Root mean square deviations (RMSD) of tryptophan 279. 6

Table S2. RMSF (Å) of binding site residues in CB1R. 7

Figure S6. System THC-cis, the biggest variations of RMSD are in loop regions (RMSD graphic), far from ligands binding site. 8

Table S3. RMSD (Å) of binding site residues in CB1R. 9

Figure S7. Energy decomposition of CB1R systems. 10

Figure S8. Influence of the (+conf) and (-conf) of the half-chair conformations in both THC and PET alters Leu-193 affinity. 11

Figure S9. Three-dimensional representation of betweenness centrality for each residue of CB1R systems. Each residue was colored according to the figure caption. 12

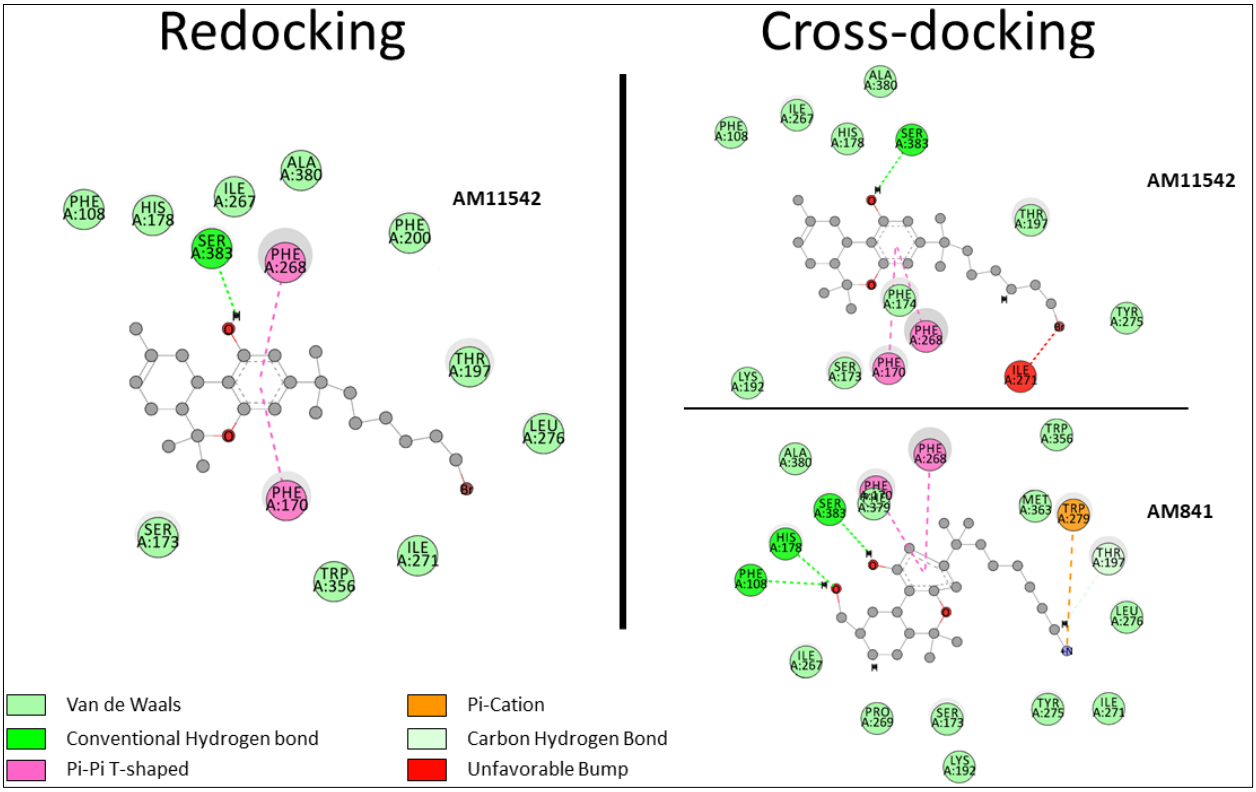

Figure S1. 2D diagrams of interactions of the best poses from redocking and cross-docking.

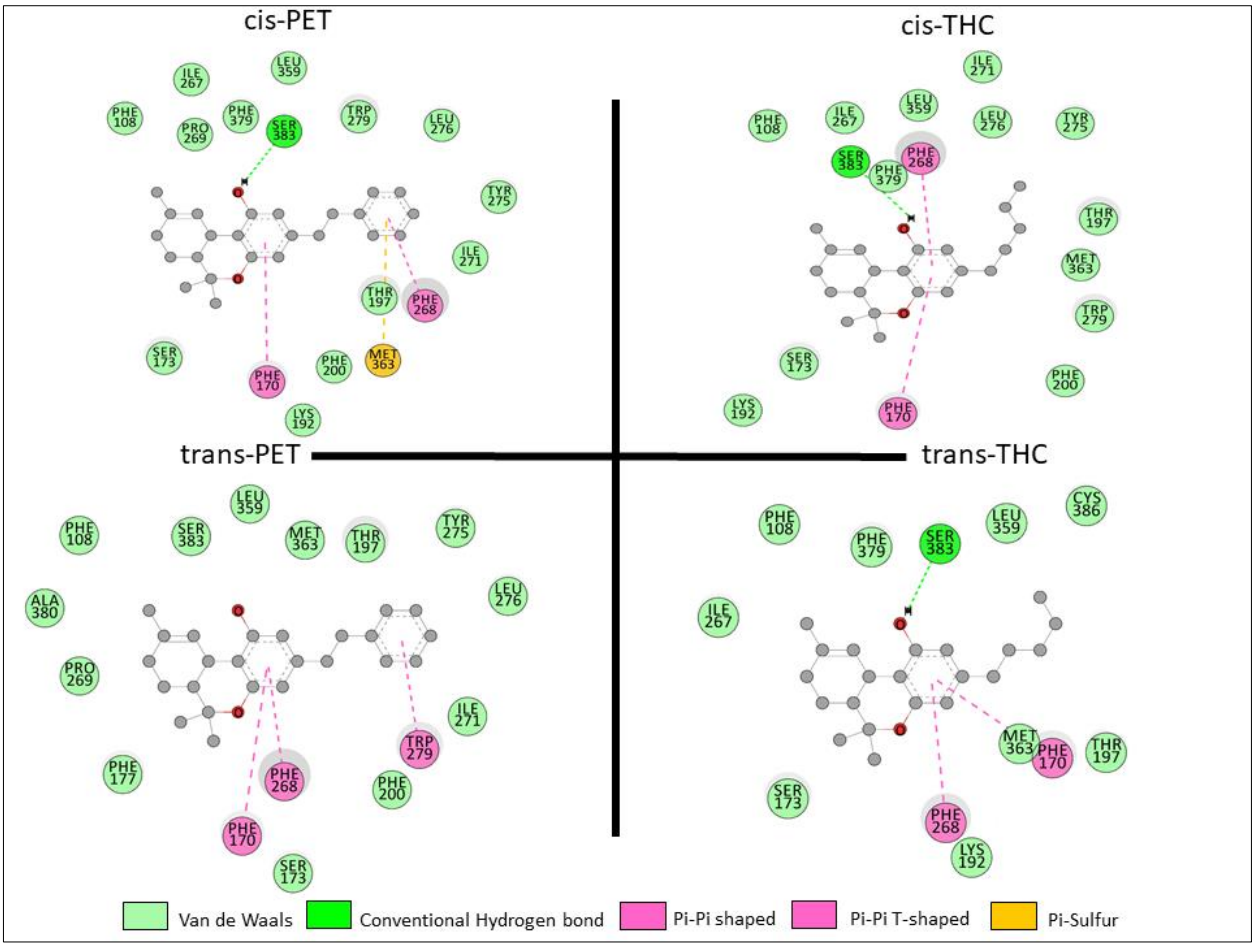

Figure S2. 2D diagrams of interactions of the best poses from docking.

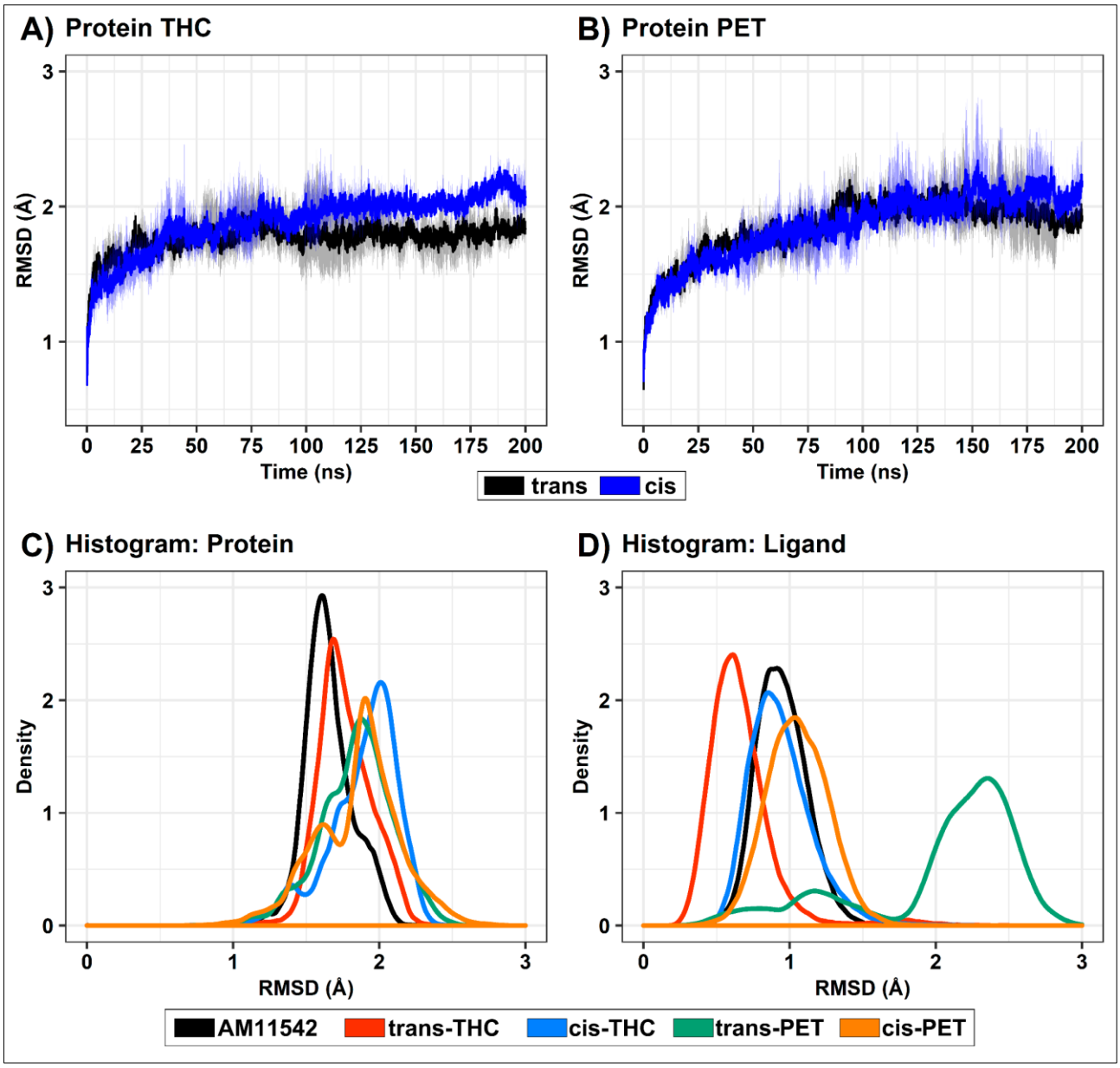

Figure S3. Root mean square deviations of CB1R systems. RMSD values of the receptor in complex with THC **(A)** and PET **(B)** considering only heavy atoms. Mean (solid lines) and confidence interval (smooth lines) of the replicates are displayed. RMSD histogram of the CB1 receptor **(C)** and ligands **(D)**. Only heavy atoms were taken into consideration for the calculations.

Table S1. Root mean square deviations (Å) of CB1R systems.

Systems	CB1R	Ligand
trans-AM11542	1.6 ± 0.2	0.9 ± 0.2
trans-THC	1.7 ± 0.2	0.7 ± 0.2
cis-THC	1.8 ± 0.2	0.9 ± 0.2
trans-PET	1.8 ± 0.2	2.0 ± 0.5
cis-PET	1.8 ± 0.3	1.0 ± 0.2

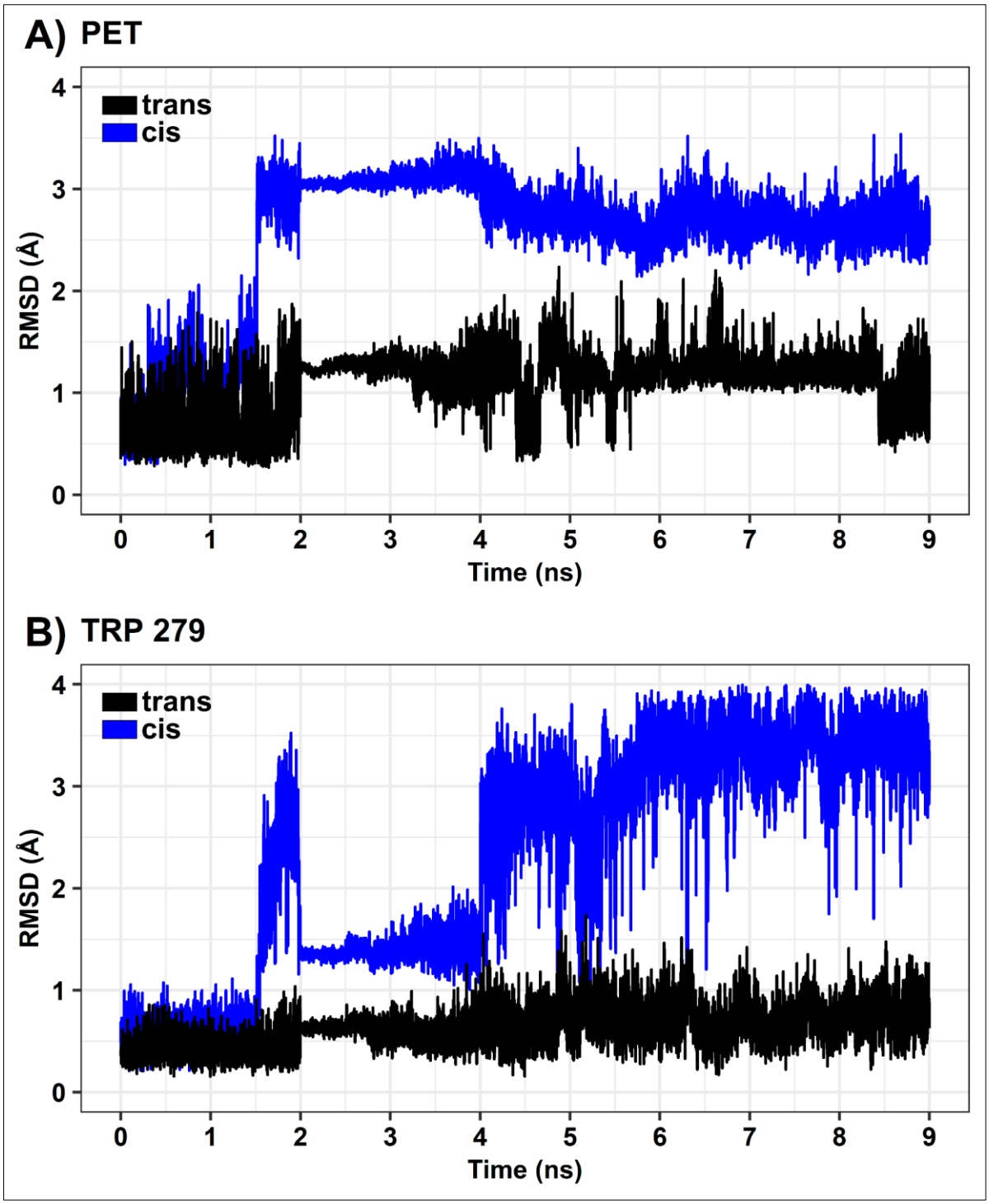

Figure S4. Root mean square deviations of PET systems during the equilibration stage (heavy atoms only). RMSD of ligand PET (A) and Tryptophan 279 (B) as a function of time. Conformations of diastereomers are depicted in black (trans) and blue (cis). Only heavy atoms were taken into consideration for the calculations.

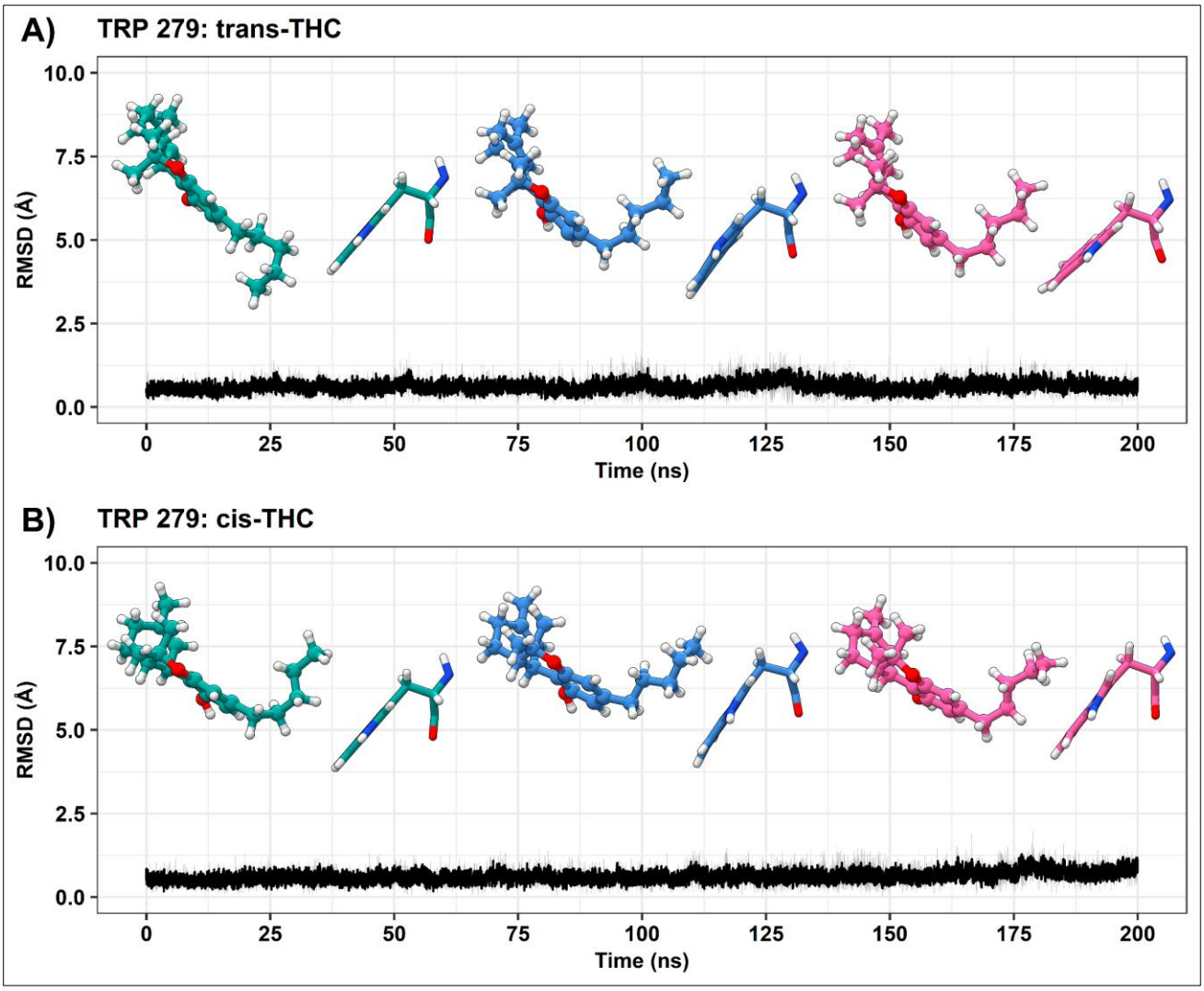

Figure S5. Root mean square deviations (RMSD) of tryptophan 279. Sticks representations of THC and Trp-279 of docking structure (green), initial production structure (blue), and the central structure resulting from clustering analysis of the last 50 ns of simulation (pink) are displayed within each plot. Mean (black lines) and confidence interval (grey lines) of the replicates are displayed. Only heavy atoms were taken into consideration for the calculations.

Table S2. RMSF (Å) of binding site residues in CB1R.

Residues	AM11542	cis-PET	trans-PET	cis-THC	trans-THC
Phe-170	0.45 ± 0.01	0.47 ± 0.01	0.44 ± 0.01	0.56 ± 0.15	0.44 ± 0.00
Phe-174	0.59 ± 0.07	0.59 ± 0.21	0.46 ± 0.04	0.53 ± 0.11	0.44 ± 0.01
Phe-177	0.54 ± 0.03	0.53 ± 0.03	0.51 ± 0.02	0.59 ± 0.03	0.49 ± 0.04
Phe-189	0.55 ± 0.01	0.56 ± 0.04	0.52 ± 0.02	0.60 ± 0.02	0.54 ± 0.03
Leu-193	0.58 ± 0.04	0.72 ± 0.01	0.58 ± 0.01	0.74 ± 0.00	0.67 ± 0.11
Val-196	0.83 ± 0.04	0.69 ± 0.07	0.69 ± 0.07	0.66 ± 0.05	0.62 ± 0.04
Phe-200	0.62 ± 0.18	0.60 ± 0.03	0.63 ± 0.08	0.92 ± 0.44	0.63 ± 0.05
Phe-268	0.53 ± 0.01	0.54 ± 0.04	0.54 ± 0.01	0.55 ± 0.00	0.54 ± 0.04
Trp-279	0.51 ± 0.01	0.61 ± 0.11	0.52 ± 0.02	0.56 ± 0.01	0.54 ± 0.00
Val-283	0.66 ± 0.05	0.69 ± 0.04	0.69 ± 0.04	0.80 ± 0.09	0.79 ± 0.12
Trp-356	0.69 ± 0.08	0.63 ± 0.07	0.64 ± 0.02	0.83 ± 0.12	0.68 ± 0.05
Leu-359	0.89 ± 0.17	0.83 ± 0.05	0.96 ± 0.05	0.96 ± 0.07	0.88 ± 0.06
Met-363	0.80 ± 0.06	0.71 ± 0.15	0.60 ± 0.02	0.91 ± 0.01	0.87 ± 0.03
Phe-379	0.59 ± 0.03	0.56 ± 0.07	0.60 ± 0.02	0.64 ± 0.13	0.53 ± 0.04
Ser-383	0.47 ± 0.03	0.47 ± 0.02	0.49 ± 0.01	0.57 ± 0.09	0.52 ± 0.03

RMSF calculations were calculated using the most typical configurations of the respective systems as a reference.

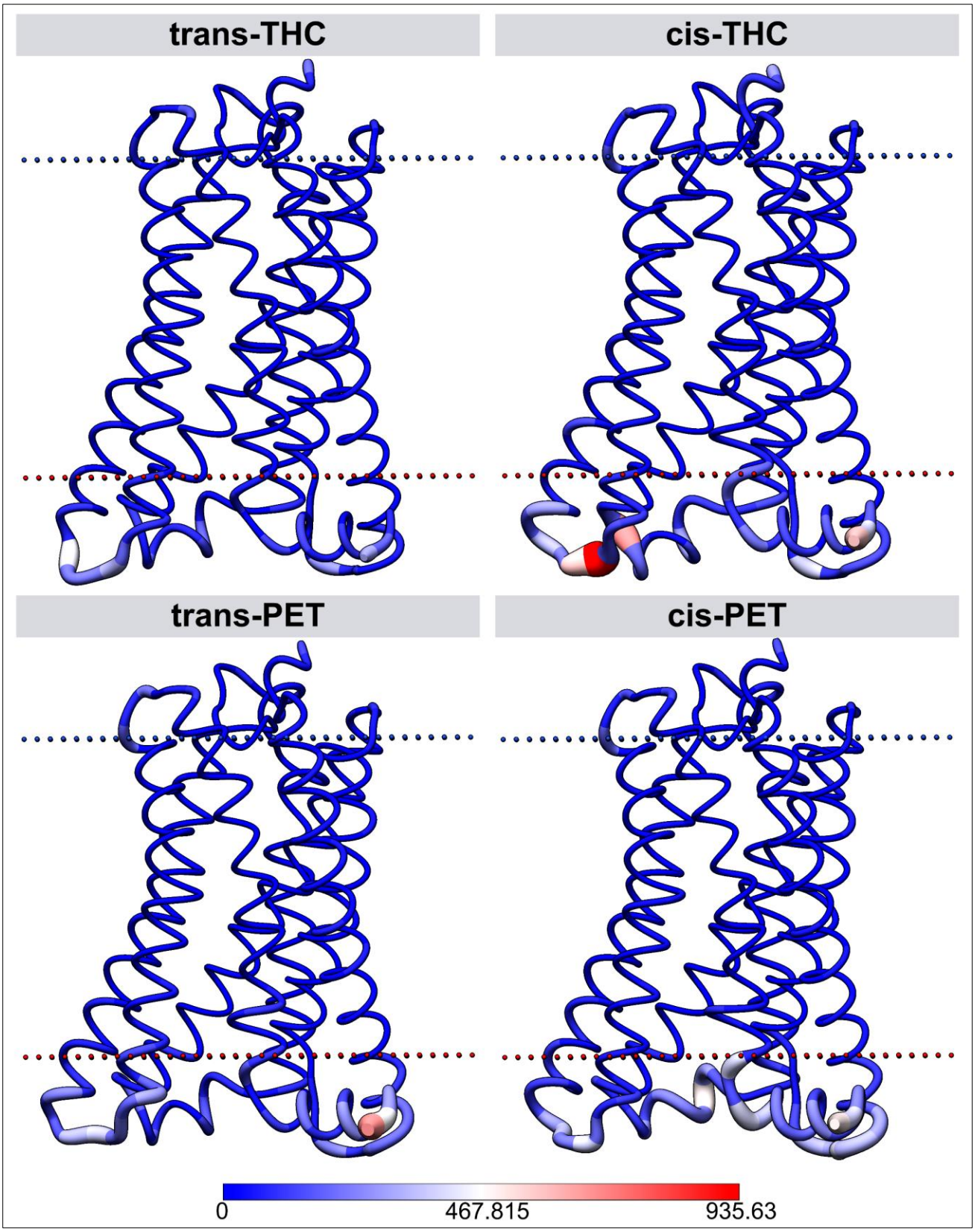

Figure S6. System THC-cis, the biggest variations of RMSD are in loop regions (RMSD graphic), far from ligands binding site.

Table S3. RMSD (Å) of binding site residues in CB1R.

	cis-THC/ trans-THC	**cis-PET/ trans-PET**	**trans-THC/ trans-PET**	**cis-THC/ cis-PET**
Ligands	1.075	0.859	0.361	0.635
Phe-170	1.280	0.782	0.692	1.400
Phe-174	1.937	0.437	0.718	2.409
Phe-177	1.548	0.664	0.707	1.561
Phe-189	0.537	0.782	0.866	1.325
Leu-193	0.557	0.390	0.416	1.237
Val-196	0.732	1.377	0.770	1.887
Phe-200	1.738	1.710	1.828	2.315
Phe-268	0.406	0.514	0.690	1.252
Trp-279	1.749	1.029	3.525	3.918
Val-283	2.748	0.914	1.397	3.035
Trp-356	1.637	0.920	1.180	1.474
Met-363	1.348	0.652	1.236	1.240
Phe-379	0.828	1.122	0.816	1.738
Ser-383	0.679	0.737	0.637	1.230

RMSD calculations considering only heavy atoms.

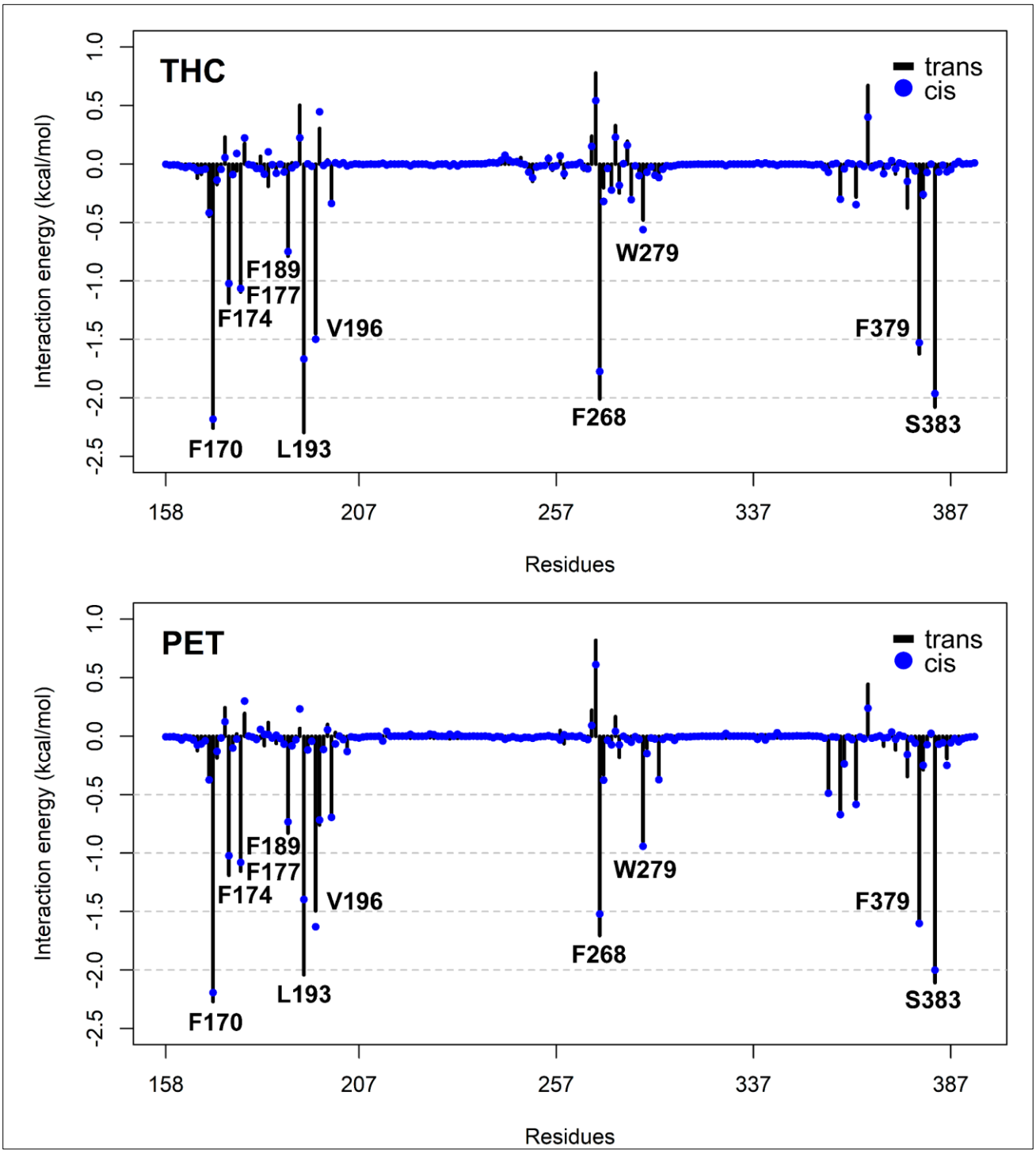

Figure S7. Energy decomposition of CB1R systems.

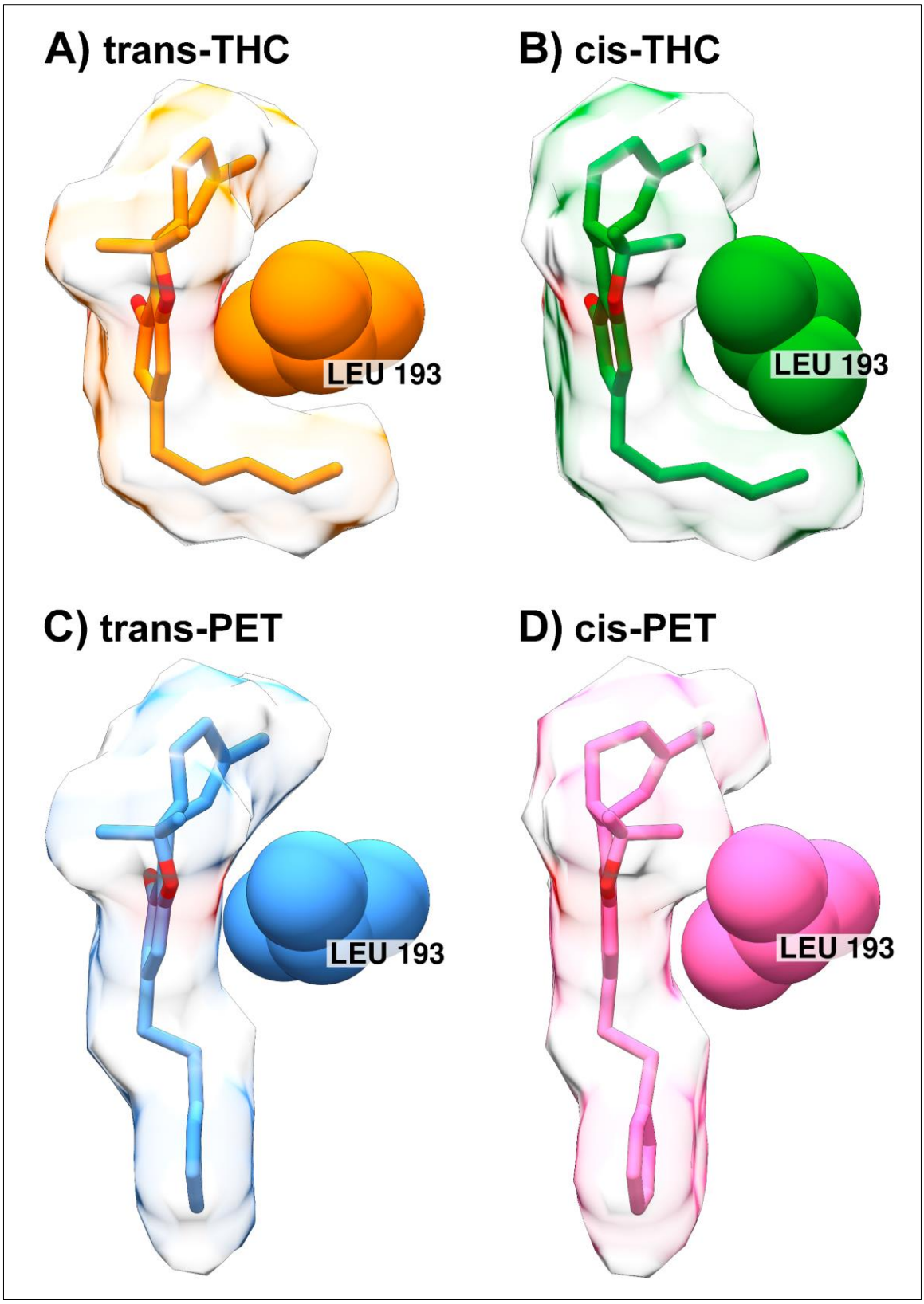

Figure S8. Influence of the (+conf) and (-conf) of the half-chair conformations in both THC and PET alters Leu-193 affinity.

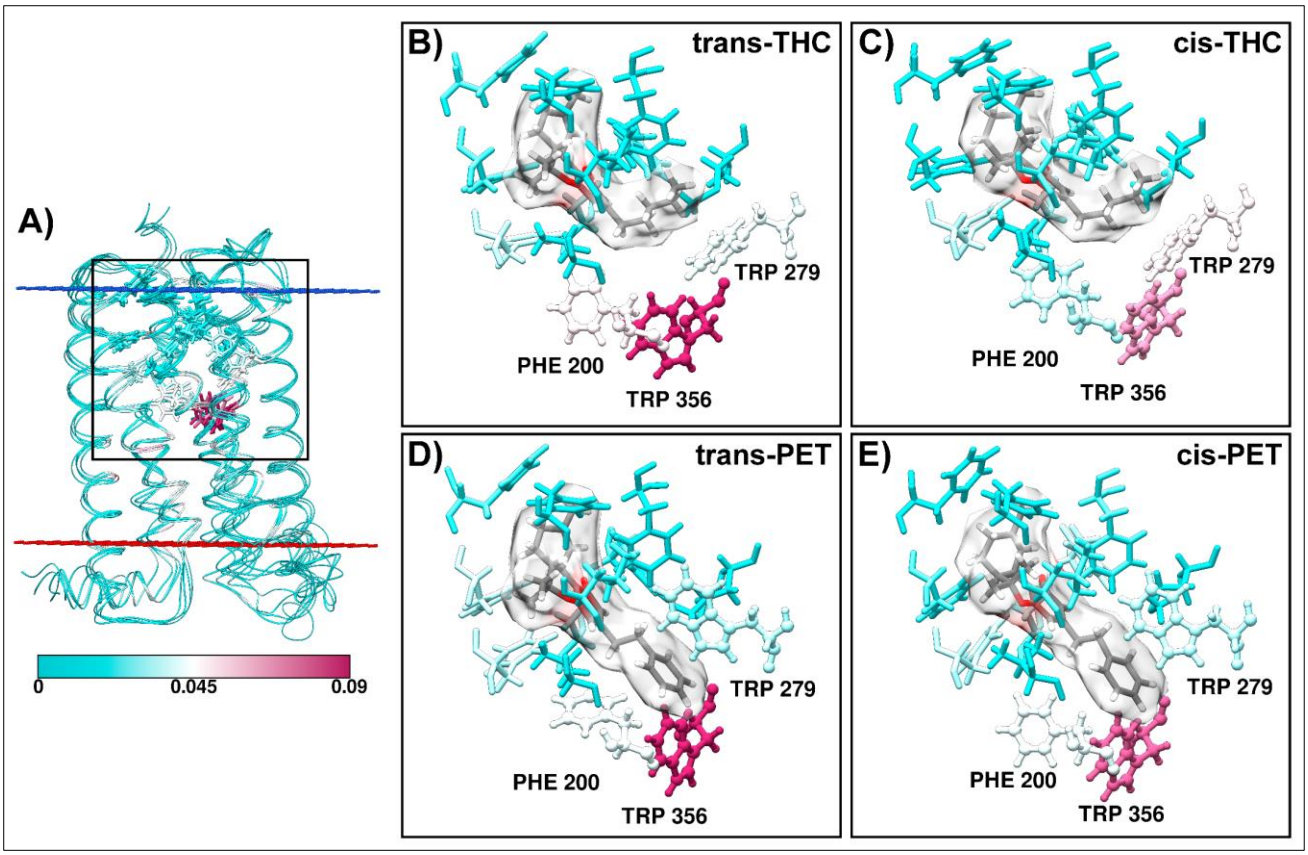

Figure S9. Three-dimensional representation of betweenness centrality for each residue of CB1R systems. Each residue was colored according to the figure caption.